# Graphene-based tunable SQUIDs

Cite as: Appl. Phys. Lett. **110**, 162602 (2017); https://doi.org/10.1063/1.4981904
Submitted: 23 December 2016 • Accepted: 05 April 2017 • Published Online: 20 April 2017

M. D. Thompson, M. Ben Shalom, A. K. Geim, et al.



# Graphene-based tunable SQUIDs

M. D. Thompson,[1,a)] M. Ben Shalom,[2] A. K. Geim,[2] A. J. Matthews,[3] J. White,[3] Z. Melhem,[3] Yu. A. Pashkin,[1] R. P. Haley,[1] and J. R. Prance[1]
[1]*Department of Physics, Lancaster University, Lancaster LA1 4YB, United Kingdom*
[2]*National Graphene Institute and School of Physics and Astronomy, The University of Manchester, Manchester M13 9PL, United Kingdom*
[3]*Oxford Instruments NanoScience, Tubney Woods, Abingdon, Oxfordshire OX13 5QX, United Kingdom*

(Received 23 December 2016; accepted 5 April 2017; published online 20 April 2017)

The superconducting proximity effect in graphene can be used to create Josephson junctions with critical currents that can be tuned using local field-effect gates. These junctions have the potential to add functionality to existing technologies; for example, superconducting quantum interference device (SQUID) magnetometers with adaptive dynamic range and superconducting qubits with fast electrical control. Here, we present measurements of graphene-based superconducting quantum interference devices incorporating ballistic Josephson junctions that can be controlled individually. We investigate the magnetic field response of the SQUIDs as the junctions are gated and as the device is tuned between symmetric and asymmetric configurations. We find a highest transfer function $\approx 300\,\mu V/\Phi_0$, which compares favorably with conventional, low temperature DC SQUIDs. With low noise readout electronics and optimised geometries, devices based on ballistic graphene Josephson junctions have the potential to match the sensitivity of traditional SQUIDs while also providing additional functionality. 
[http://dx.doi.org/10.1063/1.4981904]

When two superconductors are connected by high-quality graphene, the proximity effect allows a dissipationless current to flow through the graphene, from one superconductor to the other, over distances up to several microns.[1–12] The maximum supercurrent depends on the carrier density of the graphene, which can be controlled using the electric field effect. With appropriate fabrication techniques, it is possible to create high-quality graphene-based Josephson junctions with a tunable critical current density that can reach $\sim 3\,\mu A/\mu m$.[13] Such junctions have potential advantages in addition to their tunability: the two-dimensional nature of graphene may allow the junctions to operate in large in-plane magnetic fields; ballistic transport in the graphene can produce a non-sinusoidal current-phase relationship and a stronger response to changes in flux;[14–20] and the cleanliness of encapsulated graphene could result in lower intrinsic noise than tunnel-barrier devices. Graphene junctions have recently been used to build simple superconducting circuits including superconducting quantum interference devices (SQUIDs).[21,22] Here, we report the fabrication and characterisation of DC SQUIDs with pairs of encapsulated graphene Josephson junctions that can be tuned individually using local gates.

The layout of the devices is illustrated in Fig. 1(a). The superconductor-graphene-superconductor (SGS) junctions are formed from monolayer graphene encapsulated between two ~30 nm thick crystals of hexagonal boron nitride (hBN). The stack is fabricated on a quartz substrate by a dry-peel transfer technique[23] and then annealed at 300 °C in Ar $H_2$ for 3 h. A PMMA resist layer is patterned by electron-beam lithography, and a reactive ion etch (a mixture of $CHF_3$ and $O_2$) removes the un-masked areas of the stack. The selectivity of the etch causes narrow strips of graphene to be exposed along the contact edges. A niobium film of 50 nm thickness is then deposited through the same mask to contact the exposed graphene edges and to form the SQUID loop. The graphene in each junction is approximately 400 nm long (in the direction of current flow) and 3 $\mu$m wide. In our previous work, junctions fabricated using this technique were shown to display low contact resistance, high mobility, and ballistic transport over several microns.[13] By contrast, the junctions used in previous graphene-based SQUIDs were in the diffusive transport regime.[21,22] In the final lithography step, aluminium field-effect gates are deposited on top of the hBN covering the junctions, through a second e-beam patterned PMMA resist layer. Two SQUIDs with nominally identical junctions were fabricated and measured for this work: one with a loop area $\approx 210\,\mu m^2$ and the other with a loop area $\approx 2900\,\mu m^2$. Both SQUIDs are fabricated simultaneously using the same hBN/graphene stack. Measurements were made at 20 mK using a dilution refrigerator system equipped with an 8T superconducting solenoid and bottom loading sample exchange mechanism.[24]

Figures 1(b)–1(d) show the characteristics of the SQUID with a loop area of $\approx 210\,\mu m^2$ over a range of magnetic fields. Figure 1(b) shows the superposition of the small scale modulation of the critical current $I_C$, due to interference around the SQUID loop, and larger-scale modulation of the critical current $I_C$, which is the Fraunhofer pattern arising from interference of different current paths across the finite area of the junctions. The period of the Fraunhofer pattern is 0.6 mT, which is consistent with the junction area. The smaller-scale oscillations, magnified in Fig. 1(c), correspond to an area of $\approx 230\,\mu m^2$, similar to the loop. Small differences may be attributed to flux focussing due to the finite width of the superconducting wire. Figure 1(d) shows the

a)Author to whom correspondence should be addressed. Electronic mail: m.thompson@lancaster.ac.uk

 

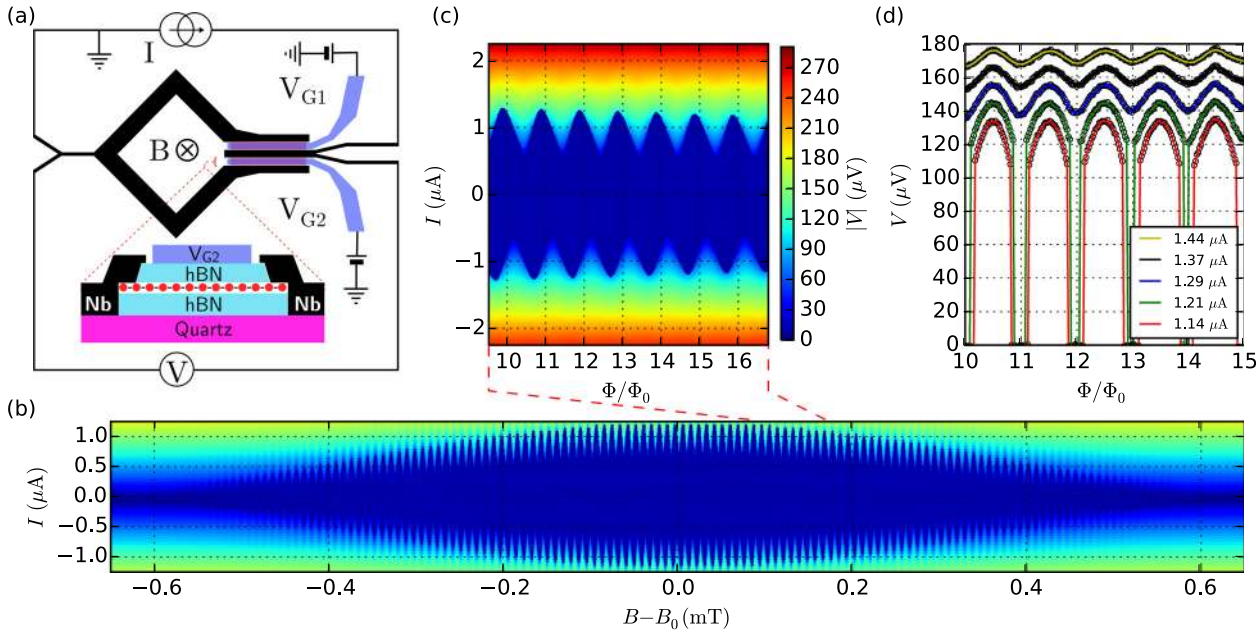


FIG. 1. Characteristics of a graphene-junction SQUID. (a) Schematic of the device. The niobium SQUID loop is shown in black and the aluminium field-effect gates in blue. The encapsulated graphene (in red) sits between the parallel niobium wires (in black) on the right side of the loop, underneath the gates. The device is measured in a current driven, four terminal configuration. The carrier density in each junction is controlled by the voltages $V_{G1}$ and $V_{G2}$. (b) Wide magnetic field sweep showing Fraunhofer interference pattern, which is caused by the finite size of the junctions, and the smaller period modulations due to interference around the SQUID loop. The colour scale is the absolute value of the DC voltage, and the scale bar is the same as in (c). Here, the junction gate voltages are both zero, and the junctions are close to their charge neutrality points. (c) Enlargement of a section of (b) showing the modulation of voltage and critical current due to changing flux in the loop. (d) Line scans from a selection of drive currents in (c). All measurements are made at 20 mK. The loop area of the SQUID is 210 $\mu$m$^2$.

DC voltage $V$ across the SQUID at several different values of the drive current $I$. At higher $I$, it displays the familiar response of a DC SQUID and transitions to superconductivity in the graphene junctions below $V \approx 110\,\mu$V. From this, we estimate the characteristic energy $eI_C^{(J)}R_N^{(J)} \gtrsim 100\,\mu$eV for the junctions, where $I_C^{(J)}$ and $R_N^{(J)}$ are the critical current and normal-state resistance of a single junction, respectively. This is consistent with our previous measurements of ballistic Nb/graphene/Nb junctions, where $I_CR_N$ was found to scale as $1/L$ for $L$ between 150 nm and 2.5 $\mu$m.[13] We have measured the temperature dependence of the critical currents and found that they do not change significantly up to a temperature of 300 mK. The critical temperature of the junctions is $T_C = eI_C^{(J)}R_N^{(J)}/k_B \sim 1$ K, and hence all the results presented here are in the low temperature limit ($T \ll T_C$).

A practical benefit of gated junctions is the ability to tune their critical currents and thereby alter the characteristics of the SQUID. Figure 2(a) shows the change in the critical current in both SQUIDs as a function of their junction gate voltages. The charge neutrality points of all four junctions, identified as the points of minimum $I_C$, are in the range of – 0.2 V to 0.5 V. At more positive voltages (n-type doping), the total critical current increases significantly in both devices. The behaviour of $I_C$ close to the charge neutrality point can also reveal the quality of the junctions: Figure 2(b) shows evidence of Fabry-Pérot oscillations in the critical current of a junction. We have studied such oscillations previously and determined that they are due to partial reflections from p–n (or n'–n) junctions that form in the graphene due to local doping by the contacts (see supplementary material of Ben Shalom *et al.*[13]) The presence of Fabry-Pérot

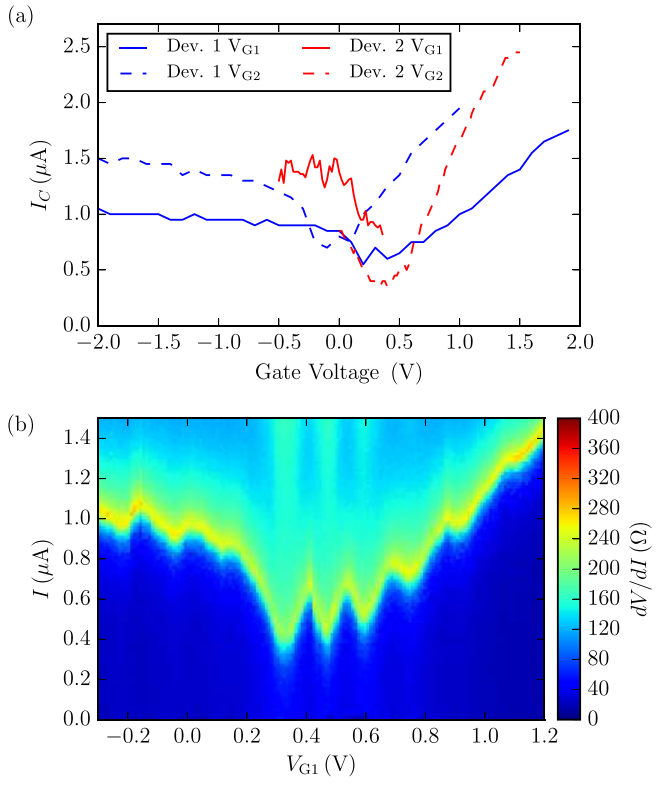


FIG. 2. Variation of SQUID critical current with gate voltage. (a) Critical current $I_C$ for both SQUIDs. (Device 1 has a 210 $\mu$m$^2$ loop and Device 2 has a 2900 $\mu$m$^2$ loop). For each measurement, the gate voltage of one junction was fixed at a value close to the charge neutrality point and $I_C$ was measured as a function of the gate voltage of the other junction. (b) Fabry-Pérot oscillations in the resistance and critical current of Device 1 as one of its junctions is gated.

oscillations demonstrates that transport in the graphene is ballistic and phase coherent on the scale of the junctions' length.[9,13]

We study the effects of tuning the junctions in a SQUID with a 2900 $\mu m^2$ loop, shown in Fig. 3. Here, $V_{G1}$ is fixed at 1.00 V and $V_{G2}$ is varied in the range of 0.5 V to 2 V. From our estimate of the gate capacitance, this corresponds to n-type doping $\sim 1.5 \times 10^{11}\,cm^{-2}$ in junction 1 and up to $4.5 \times 10^{11}\,cm^{-2}$ in junction 2. The most noticeable effect of gating is that the modulation of $I_C(\Phi)$ changes its symmetry with respect to the direction of current flow, as shown in Fig. 3(a). In a SQUID with identical junctions and a symmetric loop, the modulation of the total critical current $I_C(\Phi)$ will be symmetric with respect to the direction of current flow. However, if the inductances of the loop arms are not equal or if the junctions do not have the same critical current, then $I_C(\Phi)$ will lose this symmetry. This is because self-induced flux in the loop depends on the direction of the current when the arms of the SQUID are not identical.[25] The loop in our SQUID has an intrinsic asymmetry: one arm of the loop is approximately twice the length of the other. We find that the modulation of $I_C$ is most symmetric at $V_{G2} \approx 1.14$ V. At this point, the asymmetry in the junction critical currents cancels the asymmetry of the SQUID loop. Further increasing $V_{G2}$ increases the total $I_C$ and also reintroduces an asymmetry in the modulation of $I_C$, as expected.

The response of a SQUID to changes in magnetic flux $\Phi$ can also be controlled using the gate voltages. The response is typically quantified by the transfer function $V_\Phi = dV/d\Phi$. We measure $V_\Phi$ by modulating an external magnetic field at 4 Hz with a magnitude equivalent to 0.007 $\Phi_0$ in the loop and detecting the corresponding AC voltage across the device with a lock-in amplifier. Figure 3(b) shows $V_\Phi$ as a function of $I$ and $\Phi$ close to a point of maximum critical current. In normal operation as a magnetometer, the drive current $I$ should exceed $I_C$ at all $\Phi$, to avoid sudden transitions to the fully superconducting state. With this restriction, we find a highest transfer function of $V_\Phi = 250\,\mu V/\Phi_0$ for the data in Fig. 3(b). Over the range of gate voltages shown in Fig. 3(c), the peak transfer function can be varied by more than 40%. At high gate voltages, the peak transfer function increases to $V_\Phi = 300\,\mu V/\Phi_0$, which compares favourably with traditional low temperature DC SQUIDs.[25]

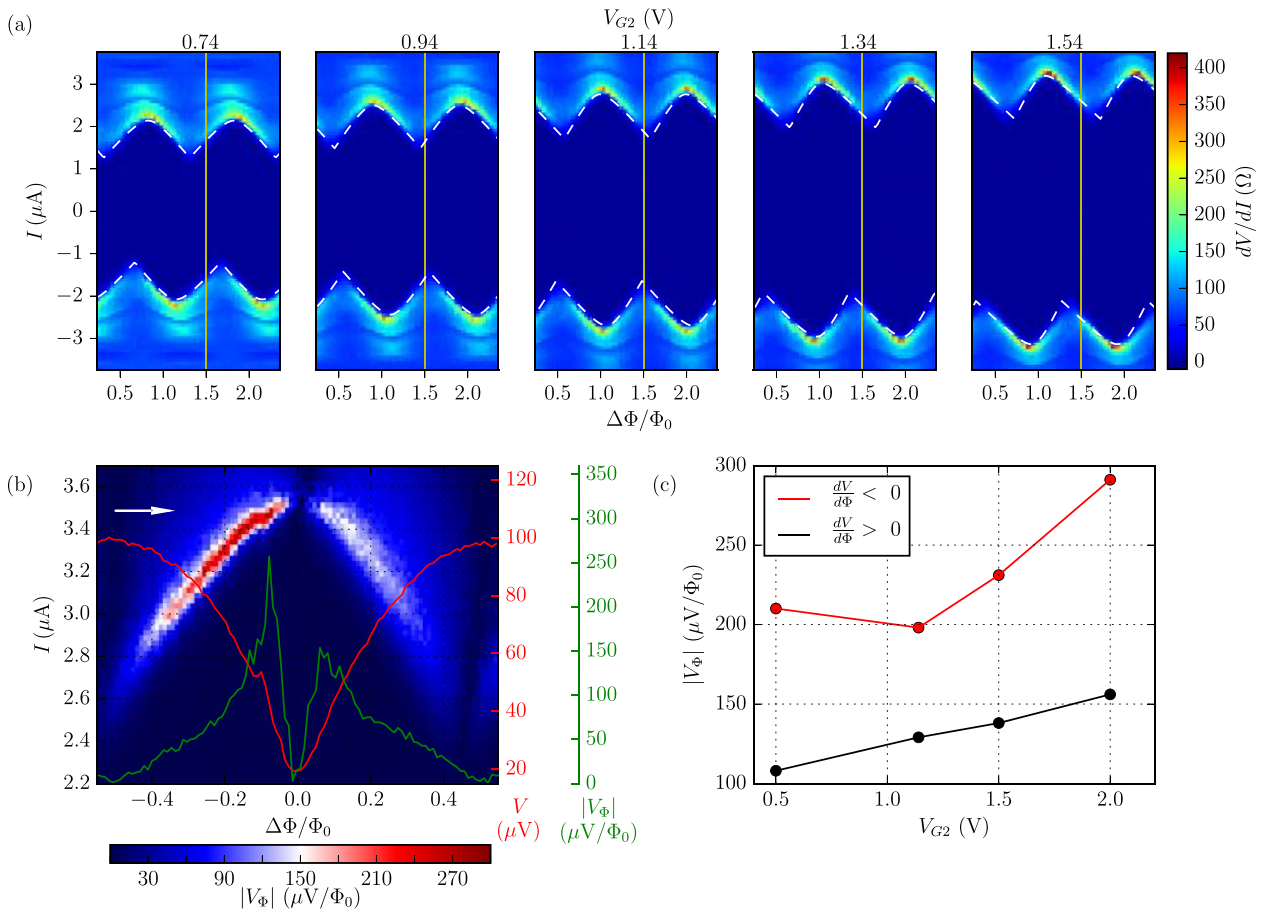


FIG. 3. Tuning a SQUID with an asymmetric loop by varying the junction critical currents. (a) Differential resistance of the SQUID, with a 2900 $\mu m^2$ loop area, as a function of gate voltage. The gate for junction 1 is fixed at $V_{G1} = 1.0$ V ($n \sim 1.5 \times 10^{11}\,cm^{-2}$) while junction 2 is varied from $V_{G2} = 0.74$ V ($n \sim 0.7 \times 10^{11}\,cm^{-2}$) to 1.54 V ($n \sim 3 \times 10^{11}\,cm^{-2}$). The modulation of the critical current $I_C(\Phi)$ is most symmetric about $I = 0$ at $V_{G2} = 1.14$ V, with greater asymmetry at higher and lower voltages. The dashed white lines show predicted values of $I_C(\Phi)$ from a numerical simulation (see main text for details). The vertical lines have been added to highlight the asymmetry in $I_C(\Phi)$. (b) Measurement of the transfer function $V_\Phi = dV/d\Phi$ over a range of flux $\Delta\Phi = 1\ \Phi_0$ at $V_{G1} = 1.0$ V and $V_{G2} = 2.0$ V. The green trace is a plot of the transfer function at the value of $I$ indicated by the white arrow. The DC voltage at the same $I$ is plotted in red. (c) Magnitude of the maximum transfer function on the positive and negative slopes of the voltage modulation as a function of $V_{G2}$. The value is always higher on the negative slope, but the difference between the two values is the lowest where the junctions are most symmetric. Lines connecting data points are guides to the eye.

A noticeable feature in Fig. 3(b) is that the magnitude of the transfer function [green trace in Fig. 3(b)] is larger on the negative slope of the voltage modulation ($dV/d\Phi < 0$) than on the positive slope ($dV/d\Phi > 0$). This asymmetry is expected when the two arms of the SQUID are not the same,[25] and in Fig. 3(c), we find a minimum asymmetry in $V_\Phi$ when the gates are tuned closest to the symmetric point.

The overall sensitivity of a SQUID to magnetic field depends on the transfer function and the noise in the measurement of voltage across the device. In our measurements, the noise is dominated by a room-temperature voltage preamplifier, limiting the sensitivity to $\approx 100\,\mu\Phi_0/\sqrt{\text{Hz}}$. However, we see no sign of intrinsic $1/f$ noise originating from the device down to a noise level of $\approx 30\,\text{nV}/\sqrt{\text{Hz}}$, and so it is likely that the intrinsic sensitivity of the device is better. To achieve a sensitivity of $1\,\mu\Phi_0/\sqrt{\text{Hz}}$ in the $2900\,\mu\text{m}^2$ device, it would be necessary to reduce the noise level below $0.27\,\text{nV}/\sqrt{\text{Hz}}$.

The critical currents of the individual junctions can be inferred by comparing the shape of $I_C(\Phi)$ in Fig. 3(a) with a numerical simulation of the device.[25] In doing so, we find that the depth of the modulation of $I_C$ in Fig. 3(a) appears to be incompatible with the expected inductance of the loop. A loop inductance of $L \sim 1$ nH is required to achieve good agreement with the data, regardless of the asymmetry of the loop, whereas an inductance $L \approx 160$ pH is expected from the device geometry (including a kinetic inductance $\sim 20$ pH[25,26]) This discrepancy can be due to the current-phase-relation (CPR) of the junctions modifying the inductance of the system.[27] When the numerical simulation is modified to use a CPR that has a smooth sawtooth shape, as expected for graphene junctions in the ballistic regime,[14–20] the inductance required to fit the data is significantly reduced. The overlayed lines in Fig. 3(a) show the predicted $I_C(\Phi)$ for a SQUID with $L = 600$ pH, a loop asymmetry of 30%, and a smoothed sawtooth CPR. For comparison, an inductance $L \approx 1.1$ nH is required to achieve a similarly good fit if the junctions are modelled with a standard, sinusoidal CPR. From the simulations shown in Fig. 3(a), we estimate that the critical current of junction 1 is $I_C^{(J1)} \approx 1.1 \pm 0.2\,\mu\text{A}$ while $I_C^{(J2)}$ varies from $0.7\,\mu\text{A}$ to $2.7\,\mu\text{A}$ as $V_{G2}$ is increased. Even when assuming a smoothed sawtooth CPR, there is still a significant discrepancy in the apparent loop inductance and the origin of this discrepancy is not known. However, the presence of a non-sinusoidal CPR is consistent with the observation of ballistic transport in Fig. 2(b) and in other junctions fabricated using the same process.[13,18,20] It also explains why the critical current is never modulated close to zero in either of our SQUIDs. This is normally due to self-induced flux in the SQUID loop; however, our devices do not have a large enough inductance for this explanation to hold (particularly the $210\,\mu\text{m}^2$ device).

In conclusion, we have demonstrated graphene superconducting quantum interference devices with independently tunable Josephson junctions. By varying the critical currents of the two junctions, the transfer function of the SQUID can be controlled. We measure a highest transfer function of $\approx 300\,\mu\text{V}/\Phi_0$, which is limited by the voltage that can be safely applied to the gates on our device. The sensitivity of the device as a magnetometer is currently limited by the noise of the room-temperature voltage preamplifier. The sensitivity would likely be improved by incorporating a cryogenic preamplifier into the measurement, and this would also allow the intrinsic noise of the SGS junctions to be investigated. The current results demonstrate the potential of SGS junctions to add functionality to SQUIDs and indicate the future optimisations that are required to approach state-of-the-art magnetic field sensitivity in a graphene-based SQUID magnetometer.

We thank V. I. Fal'ko for useful discussions. This project has received funding from InnovateUK, UK EPSRC and the European Union's Horizon 2020 research and innovation programme under Grant agreement No. 696656. Yu.A.P. acknowledges support by the Royal Society (WM110105). J.R.P. acknowledges support of the Marie Curie People Program (REA Grant agreement No. 618450).

[1] H. B. Heersche, P. Jarillo-Herrero, J. B. Oostinga, L. M. K. Vandersypen, and A. F. Morpurgo, Nature **446**, 56 (2007).
[2] X. Du, I. Skachko, and E. Andrei, Phys. Rev. B **77**, 184507 (2008).
[3] C. Ojeda-Aristizabal, M. Ferrier, S. Guéron, and H. Bouchiat, Phys. Rev. B **79**, 165436 (2009).
[4] I. V. Borzenets, U. C. Coskun, S. J. Jones, and G. Finkelstein, Phys. Rev. Lett. **107**, 137005 (2011).
[5] K. Komatsu, C. Li, S. Autier-Laurent, H. Bouchiat, and S. Guéron, Phys. Rev. B **86**, 115412 (2012).
[6] U. C. Coskun, M. Brenner, T. Hymel, V. Vakaryuk, A. Levchenko, and A. Bezryadin, Phys. Rev. Lett. **108**, 097003 (2012).
[7] N. Mizuno, B. Nielsen, and X. Du, Nat. Commun. **4**, 2716 (2013).
[8] J.-H. Choi, G.-H. Lee, S. Park, D. Jeong, J.-O. Lee, H.-S. Sim, Y.-J. Doh, and H.-J. Lee, Nat. Commun. **4**, 2525 (2013).
[9] V. E. Calado, S. Goswami, G. Nanda, M. Diez, A. R. Akhmerov, K. Watanabe, T. Taniguchi, T. M. Klapwijk, and L. M. K. Vandersypen, Nat. Nanotechnol. **10**, 761 (2015).
[10] M. T. Allen, O. Shtanko, I. C. Fulga, A. R. Akhmerov, K. Watanabe, T. Taniguchi, P. Jarillo-Herrero, L. S. Levitov, and A. Yacoby, Nature Phys. **12**, 128 (2016).
[11] I. V. Borzenets, F. Amet, C. T. Ke, A. W. Draelos, M. T. Wei, A. Seredinski, K. Watanabe, T. Taniguchi, Y. Bomze, M. Yamamoto, S. Tarucha, and G. Finkelstein, Phys. Rev. Lett. **117**, 237002 (2016).
[12] C. T. Ke, I. V. Borzenets, A. W. Draelos, F. Amet, Y. Bomze, G. Jones, M. Craciun, S. Russo, M. Yamamoto, S. Tarucha, and G. Finkelstein, Nano Lett. **16**, 4788 (2016).
[13] M. Ben Shalom, M. J. Zhu, V. I. Fal'ko, A. Mishchenko, A. V. Kretinin, K. S. Novoselov, C. R. Woods, K. Watanabe, T. Taniguchi, A. K. Geim, and J. R. Prance, Nature Phys. **12**, 318 (2015).
[14] M. Titov and C. W. J. Beenakker, Phys. Rev. B **74**, 041401 (2006).
[15] A. M. Black-Schaffer and S. Doniach, Phys. Rev. B **78**, 024504 (2008).
[16] I. Hagymási, A. Kormányos, and J. Cserti, Phys. Rev. B **82**, 134516 (2010).
[17] A. M. Black-Schaffer and J. Linder, Phys. Rev. B **82**, 184522 (2010).
[18] P. Rakyta, A. Kormányos, and J. Cserti, Phys. Rev. B **93**, 224510 (2016).
[19] C. D. English, D. R. Hamilton, C. Chialvo, I. C. Moraru, N. Mason, and D. J. Van Harlingen, Phys. Rev. B **94**, 115435 (2016).
[20] H. Meier, V. I. Fal'ko, and L. I. Glazman, Phys. Rev. B **93**, 184506 (2016).
[21] C. Girit, V. Bouchiat, O. Naaman, Y. Zhang, M. F. Crommie, A. Zettl, and I. Siddiqi, Nano Lett. **9**, 198 (2009).
[22] K. Tsumura, M. Ohsugi, T. Hayashi, E. Watanabe, D. Tsuya, S. Nomura, and H. Takayanagi, J. Phys. Chem. Solids **400**, 042064 (2012).
[23] A. V. Kretinin, Y. Cao, J. S. Tu, G. L. Yu, R. Jalil, K. S. Novoselov, S. J. Haigh, A. Gholinia, A. Mishchenko, M. Lozada, T. Georgiou, C. R. Woods, F. Withers, P. Blake, G. Eda, A. Wirsig, C. Hucho, K. Watanabe, T. Taniguchi, A. K. Geim, and R. V. Gorbachev, Nano Lett. **14**, 3270 (2014).
[24] G. Batey, S. Chappell, M. Cuthbert, M. Erfani, A. Matthews, and G. Teleberg, Cryogenics **60**, 24 (2014).
[25] J. Clarke and A. I. Braginski, *The SQUID Handbook* (Wiley, 2004), Vol. **1**.
[26] R. Meservey and P. M. Tedrow, J. Appl. Phys. **40**, 2028 (1969).
[27] A. A. Golubov, M. Y. Kupriyanov, and E. Il'ichev, Rev. Mod. Phys. **76**, 411 (2004).